Electronic Supplementary Information

Surface and Bulk Reconstruction of CoW Sulfides During pH-Universal Electrocatalytic Hydrogen Evolution

Ke Fan[a,*,†], Haiyuan Zou[b,c,†], N. V. R. Aditya Dharanipragada[d], Lizhou Fan[e], A. Ken Inge[d], Lele Duan[c], Biaobiao Zhang[e,*], Licheng Sun[a,e,f,*]

[a] *State Key Laboratory of Fine Chemicals, Institute of Artificial Photosynthesis, DUT-KTH Joint Education and Research Centre on Molecular Devices, Institute for Energy Science and Technology, Dalian University of Technology, 116024, Dalian, China*

[b] *School of Chemistry and Chemical Engineering, Harbin Institute of Technology, Harbin 150001, China.*

[c] *Department of Chemistry, Shenzhen Grubbs Institute and Guangdong Provincial Key Laboratory of Energy Materials for Electric Power, Southern University of Science and Technology, Shenzhen, 518055, China*

[d] *Department of Materials and Environmental Chemistry, Stockholm University, 10691 Stockholm, Sweden*

[e] *Department of Chemistry, KTH Royal Institute of Technology, 10044, Stockholm, Sweden*

[f] *Center of Artificial Photosynthesis for Solar Fuels, School of Science, Westlake University, 310024 Hangzhou, China*

† *These authors contributed equally to this paper*

**Emails: kefan@kth.se; biaobiao@kth.se; lichengs@kth.se*

Methods

Material synthesis: SiO_2 spheres with diameter of ~ 200 nm were synthesized via a previously reported method. A series of mixed-metal sulfides formulated as $Co_zW_yS_x$ ($y + z = 1$) were synthesized through a direct chemical synthesis method. Briefly, 0.4 g SiO_2 was dispersed in 0.93 g ethylene glycol, followed by stirring and sonicating under room temperature to form a colloidal disperse. Then, solutions of metal precursor complexes were prepared by dissolving the appropriate ratio of metal complexes in 5 mL distilled water to achieve an overall 6% w/w solution. Precursor solutions used contain cobaltous nitrate hexahydrate ($Co(NO_3)_2{\cdot}6H_2O$) and ammonium tungstate hydrate ($(NH_4)_6W_7O_{24}{\cdot}6H_2O$). The precursor solution was poured into the SiO_2 colloidal disperse above, and stirred at 120 °C to remove the solvent. The gained bulk solids were transferred into a tube furnace under a flow of CS_2 gas and maintained at 400 °C for 3 h with a ramping rate of 3 °C min^{-1}. The final product was then leached in hydrofluoric acid to remove the SiO_2 spheres, followed by washing with water drying at 60 °C in a vacuum oven.

Electrode preparation. For the test, 4 mg catalyst was suspended in a mixture of 800 μL distilled water and 200 μL ethanol with 20 μL Nafion solution (5 wt% in ethanol) to form a uniform ink by ultrasonic treatment. Then 5 μL of the ink was spread onto a freshly polished glassy carbon (GC, 3 mm diameter), yielding an average mass loading of around 0.21 mg cm^{-2}.

Hydrogen evolution reaction (HER) electrocatalysis. All electrochemical measurements were evaluated on a CHI 760D electrochemical analyzer (Shanghai Chenhua Instrument Crop., China) using a standard three-electrode system, where the catalysts load on GC as the working electrode, a graphite rod as the counter electrode

and a Ag/AgCl electrode (saturated KCl-filled) as the reference electrode, respectively. 1.0 M KOH, 0.5 M H_2SO_4 and 1 M phosphate buffered solutions (PBS, pH = 7) were served as the alkaline, acidic and neutral electrolytes, respectively. Potentials measured against a Ag/AgCl electrode were referenced to a reversible hydrogen electrode (RHE), E_{RHE} (V) = $E_{Ag/AgCl}$ + 0.059pH + 0.197. Linear sweep voltammetry (LSV) curves were initially conducted for several times until stable curves obtained, after which the other electrochemical tests were followed. Polarization curves were obtained using the stable LSV with a scan rate of 5 mV s^{-1}. Tafel slopes were estimated by plotting overpotential η against log (*J*) *via* polarization curves. The LSV curves and Tafel plots in this study are *i*R-compensated, where the values of R are determined by electrochemical impedance spectra (~ 7 to 11 Ω). The chronpotentiometric measurement was conducted at a current density of 10 mA cm^{-2} on the working electrode.

Structure Characterizations: All the samples were stored in vacuum before the characterizations. The morphologies of all the synthesized samples were confirmed by a JMS-7500 field emission scanning electron microscopy (FESEM, JEOL, Japan) with an energy-dispersive spectroscopy (EDS) facility. TEM, HAADF-STEM and HRTEM were operated at a JEM-2100F electron microscope (JEOL, Japan). XRD patterns were carried out on a D/MAX-RB X-ray diffractometer (Rigaku, Japan). XPS measurements were performed on an XPS (XSAM800) with Al Kα source (1486.6 eV), and the binding energy was referenced to C1s peak at 284.8 eV from adventitious carbon. The specific surface areas were tested on an ASAP 2020 (Micrometritics instrument, USA) nitrogen adsorption apparatus, and calculated by nitrogen adsorption-desorption isotherms using the Brunauer-Emmett-Teller (BET) method.

X-ray absorption spectroscopy (XAS) measurement. The extended X-ray absorption fine structure (EXAFS) measurements were performed at the Co-K (7709 eV) and W-LIII (10,206 eV) edges at P-64, Petra III, DESY. The transmission measurements at the Co-K edge were performed with simultaneous measurements of samples along with Co foil as reference. The W-LIII measurements were carried out in fluorescence mode.

The data treatment steps of pre-edge and post-edge background removal to obtain normalized spectra were performed using EXAFSPAK software package,[1] subsequently followed by Fourier transformation and data fitting. The k^3-weighted EXAFS oscillations were analysed by nonlinear least-squares fits of the data to the EXAFS equation. The model parameters: mean number of neighbors, $\boldsymbol{N}$, mean distances, $\boldsymbol{d}$ (Å), and Debye-Waller coefficients, $\boldsymbol{\sigma^2}$ (Å^2), and many-body amplitude reduction factor, S_0^2 were refined. The theoretical phases and amplitudes used in the refinements were calculated using FEFF6.[2] General errors on coordination numbers and Debye–Waller factors estimated were to be within 15-25%. The mean number of distances were refined and optimized, however were fixed in the last refinements to obtain optimized final refinements. Errors in distances are in the order of ±0.01 Å. The "weighted *F*-factor" was used to determine the goodness of fit, a parameter generated by the EXAFSPAK software package. This represents χ^2 weighted by the magnitude of the data, and were typically lying between 0.30 and 0.10 suggesting a reasonable to good fit .[3,4]

In addition to the Fourier transform structure modelling, a Cauchy wavelet transform (CCWT) analysis was performed. This facilitates simultaneous data resolution in k and R spaces. A simplified EXAFS equation can be expressed as:

$$\chi(k) = \sum_j \frac{N_j S_o^2 f_j(k) e^{\frac{-2R_j}{\lambda}} e^{-2k^2\sigma_j{}^2}}{kR^2} sin[2kR_j + \delta_j(k)]$$

N: Mean number of neighbors,

R: Mean distances (Å),

σ^2: Debye-Waller coefficients (Å^2),

f(k): Many-body scattering amplitude,

δ(k): Mean-square disorder of neighbour distance,

S_0^2: Many body amplitude reduction factor.

The scattering amplitude f(k) and phase shift δ(k) depend on atomic mass (Z). Hence, the scattering amplitudes are localized to a specific k-range within k-space depending on the absorber-backscatterer. In conventional EXAFS modelling the FT magnitude in R-space is dependent on frequency of the k-space signal but independent of location. Hence, the nature of atomic species cannot be accurately distinguished when located at the same radial distance. However, the simultaneous resolution of k and R-space in CCWT provides qualitative and relatively more accurate information on the type of atomic species.

The scattering amplitude shifts to a higher k-range with increasing atomic number. This results in localization of atomic species in a specific k-range.[5] This phenomenon is shown in Fig. S1. The effective backscattering amplitude of W, Co and S with respect to a central absorber W show that the f(k) of W-W shows a maximum at intermediate k-range and this value increases with at a higher k-ranges. The W-S and W-Co show a maximal amplitude in low k-ranges and show a decline in the amplitudes thereafter (Fig. S1a). A similar trend with respect to Co as absorber and W, S and Co

as neighbouring atoms is shown in Fig. S1b. Thus, the heavy elements such as W show maxima at higher k-ranges, with a secondary maximum at intermediate k-ranges (4 – 8 $Å^{-1}$).

Hence, it is possible to qualitatively distinguish between elements such as Co and W. The shape of the wavelet is also influenced by location of atomic species and can result in different shapes of the wavelet transform.

The comparison of CCWT (Fig. S2) of metallic W and Co foils indicate W metallic species with a peak maximum at relatively higher k-range values in comparison to Co. The CCWT contour plots were generated using the computation MATLAB code by Muñoz et al. .[6,7] The conclusions from CCWT analysis in the present study are qualitative. However, the quantitative structural parameters were obtained from the Fourier transform EXAFS modelling. Both FT modelling and CCWT were used to identify the type of atomic species in the samples.

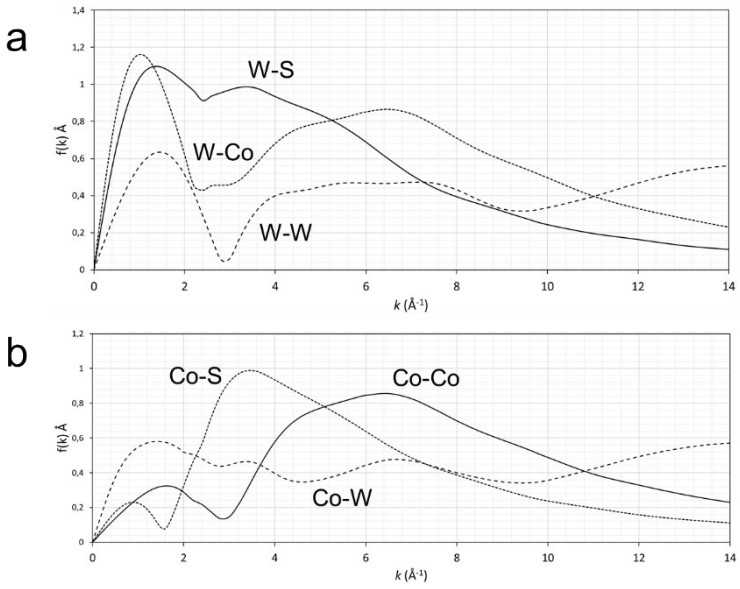

Fig. S1. (a) The scattering amplitude f(k) of W-W, W-Co and W-S, here W is the central absorbing atom. (b) The Co-W, Co-S, and Co-Co scattering amplitude f(k) with Co as the central absorbing atom.

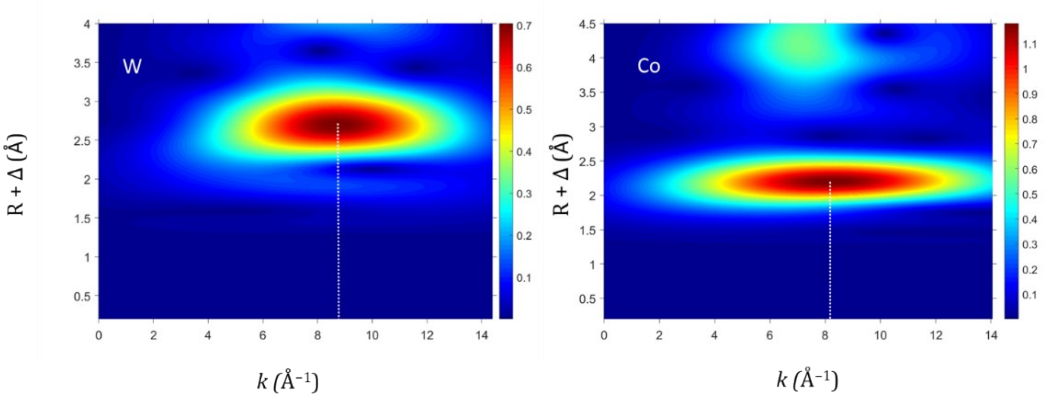

Fig. S2: The comparison of amplitude maxima in W (left) and Co-foils (right).

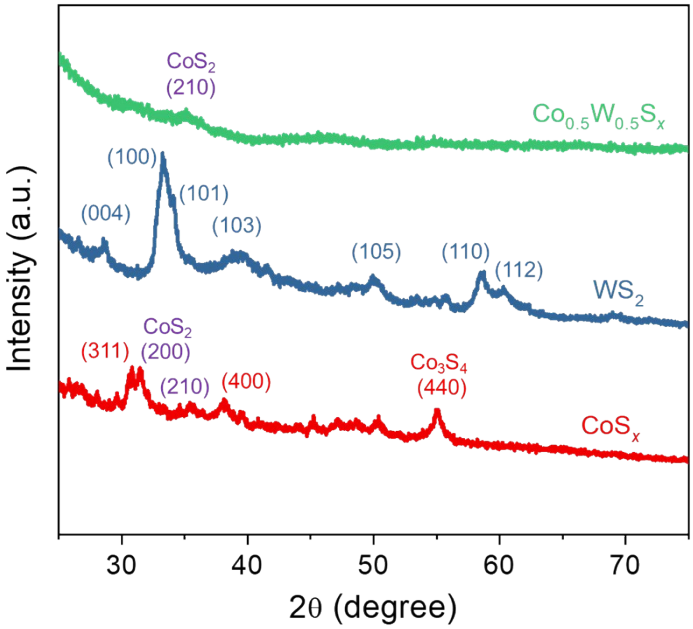

Fig. S3. XRD patterns of sulfides in this study. The red, purple and blue plane (hkl) index numbers correspond to Co_3S_4 (JCPDS # 42-1448), CoS_2 (JCPDS # 65-3322) and WS_2 (JCPDS # 08-0237), respectively.

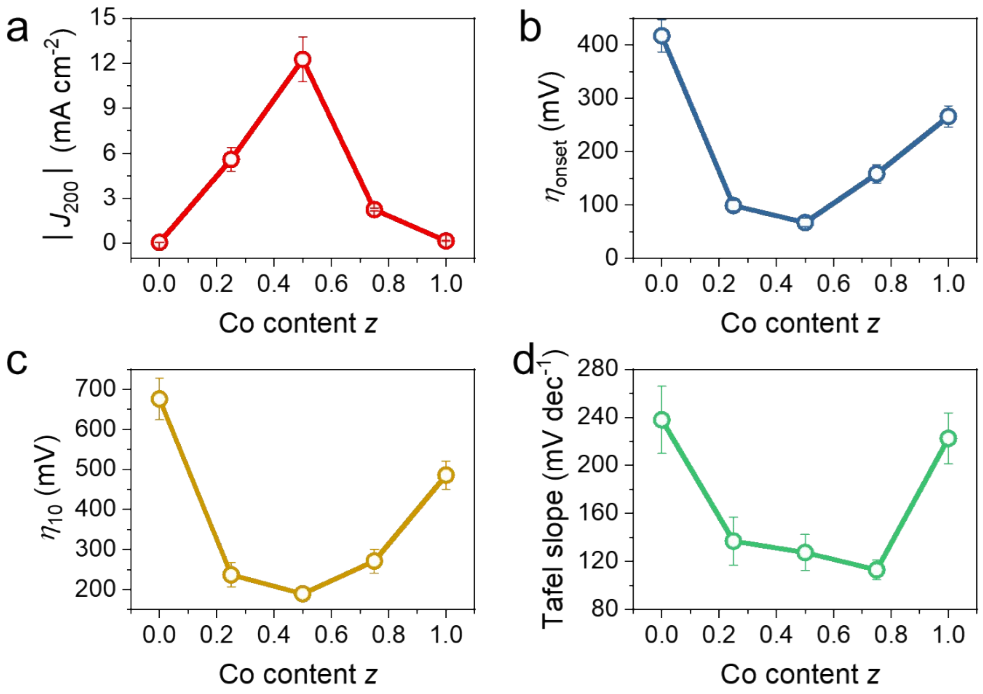

Fig. S4. (a) J_{200}, (b) η_{onset}, (c) η_{10} and (d) Tafel slope values of CoW sulfides for HER in 1 M KOH (alkaline).

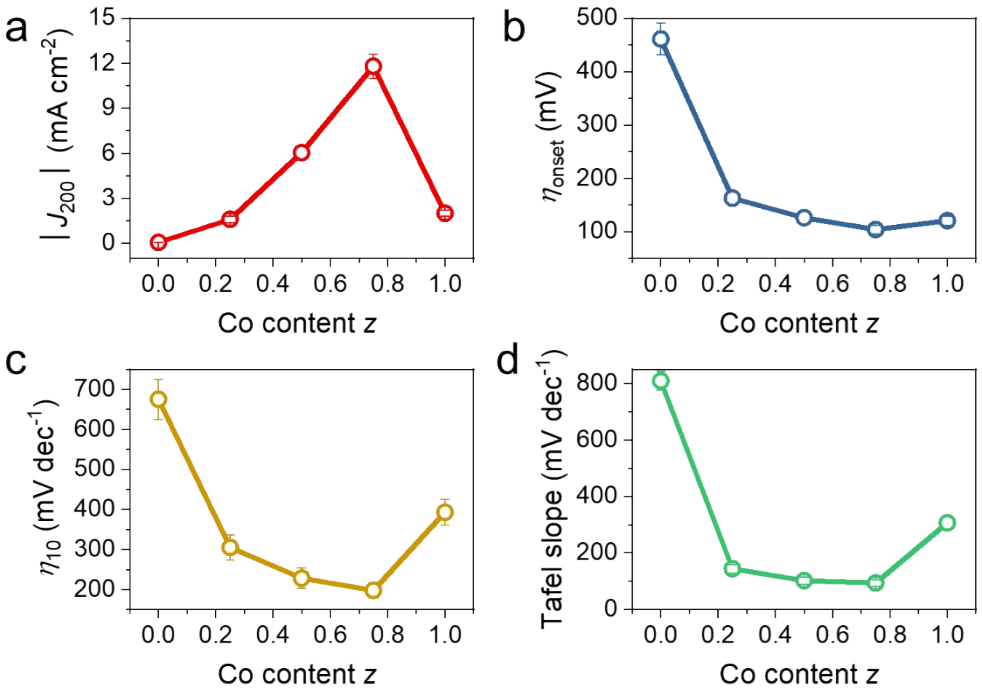

Fig. S5. (a) J_{200}, (b) η_{onset}, (c) η_{10} and (d) Tafel slope values of CoW sulfides for HER in 1 M PBS (neutral).

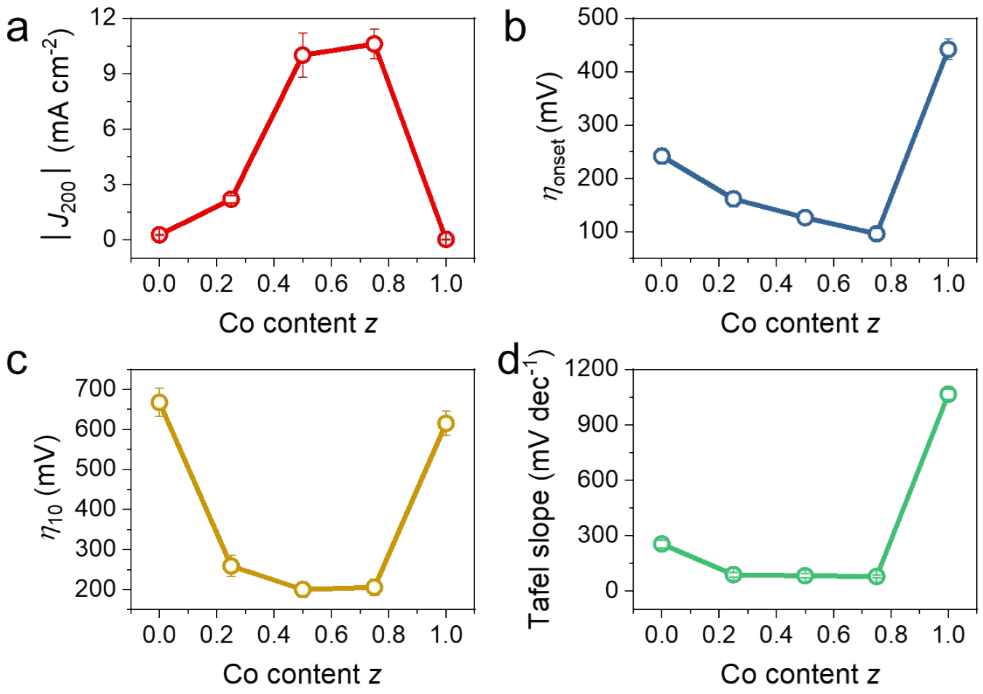

Fig. S6. (a) J_{200}, (b) η_{onset}, (c) η_{10} and (d) Tafel slope values of CoW sulfides for HER in 0.5 M H_2SO_4 (acidic).

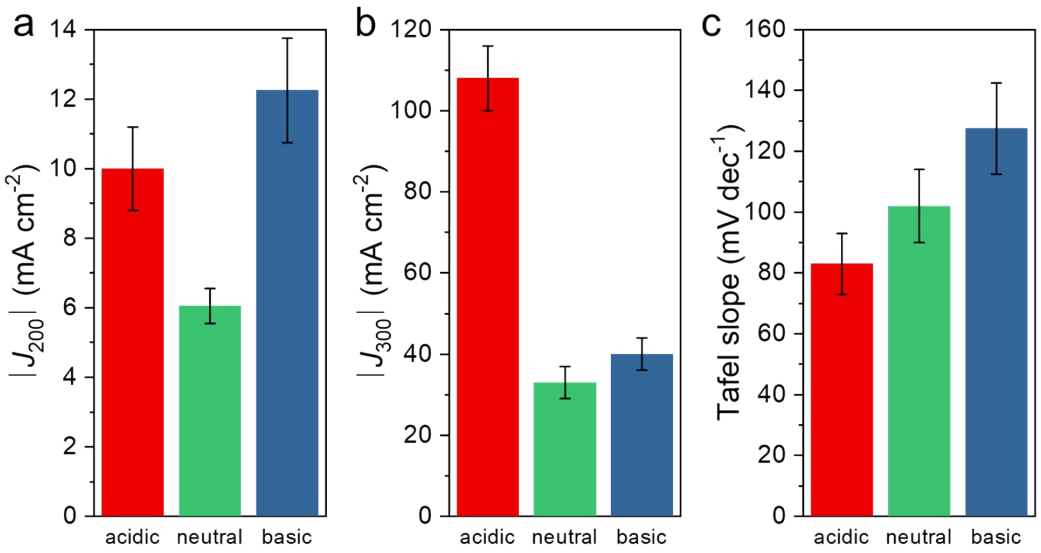

Fig. S7. The direct comparison of (a) J_{200}, (b) J_{300} (the current density at 300 mV overpotential) and (c) Tafel slope values of $Co_{0.5}W_{0.5}S_x$ in different electrolytes.

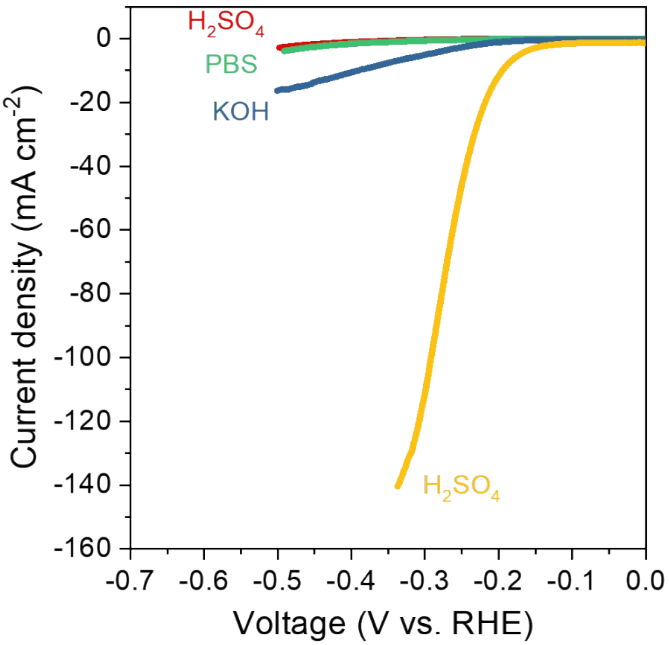

Fig. S8. HER performance in pH-universal electrolytes of $Co_{0.5}W_{0.5}S_x$ prepared without SiO_2 sphere template in the preparation (red, green and blue lines). As the comparison, the acidic HER performance of $Co_{0.5}W_{0.5}S_x$ prepared with SiO_2 sphere template in the preparation is also shown (yellow line).

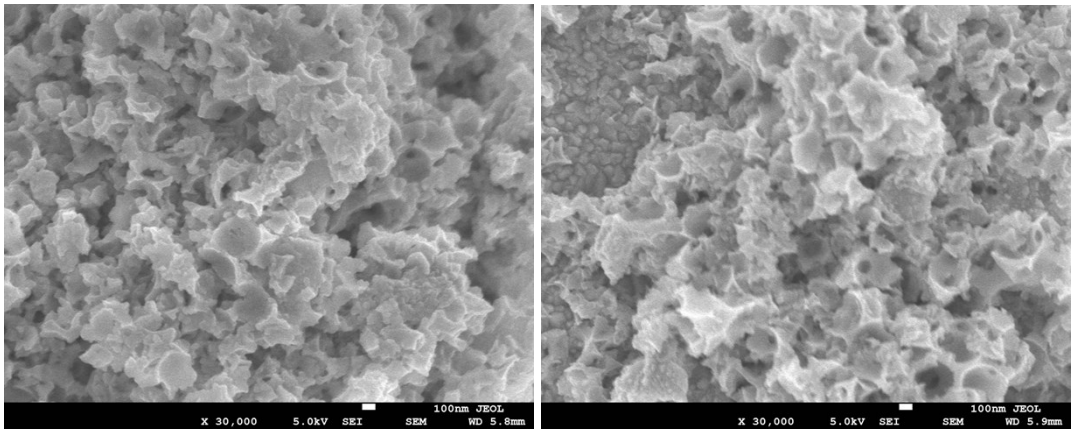

Fig. S9. SEM images of $Co_{0.5}W_{0.5}S_x$ after HER in PBS (left) and H_2SO_4 (right).

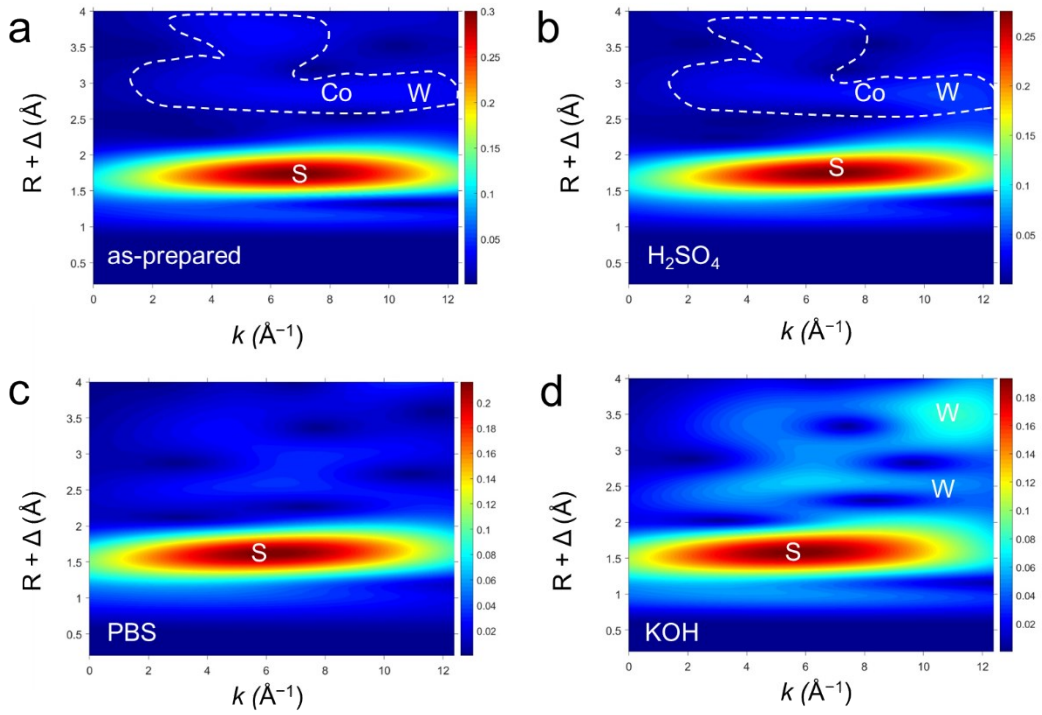

Fig. S10. The Co-K wavelet transforms of (a) the as-prepared $Co_{0.5}W_{0.5}S_x$ and $Co_{0.5}W_{0.5}S_x$ after HER in (b) H_2SO_4, (c) PBS and (d) KOH electrolytes.

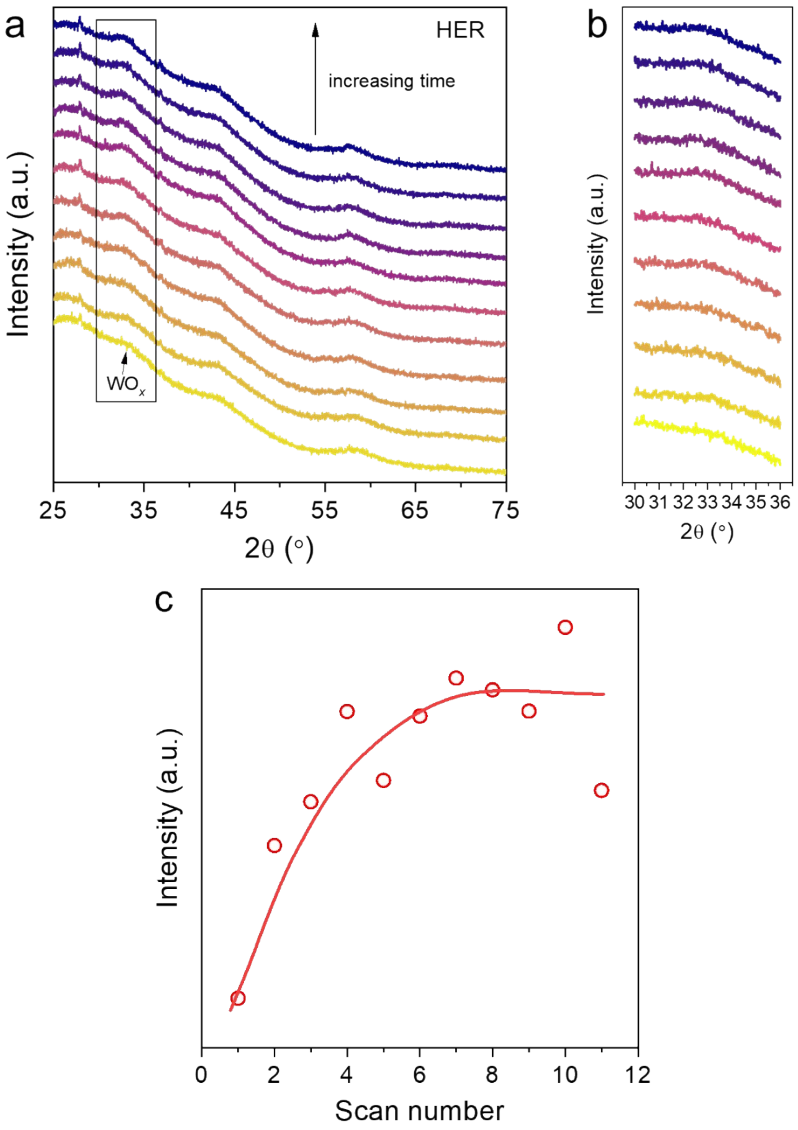

Fig. S11. (a) The operando XRD of $Co_{0.5}W_{0.5}S_x$ under the fixed current density of -2 mA cm^{-2} for HER. (b) The magnified peaks indexed to WOx in (a). (c) The change of the peak intensity indexed to WO_x (the baselines are subtracted) with the scan number of the XRD. The red curve line is used to guide eyes.

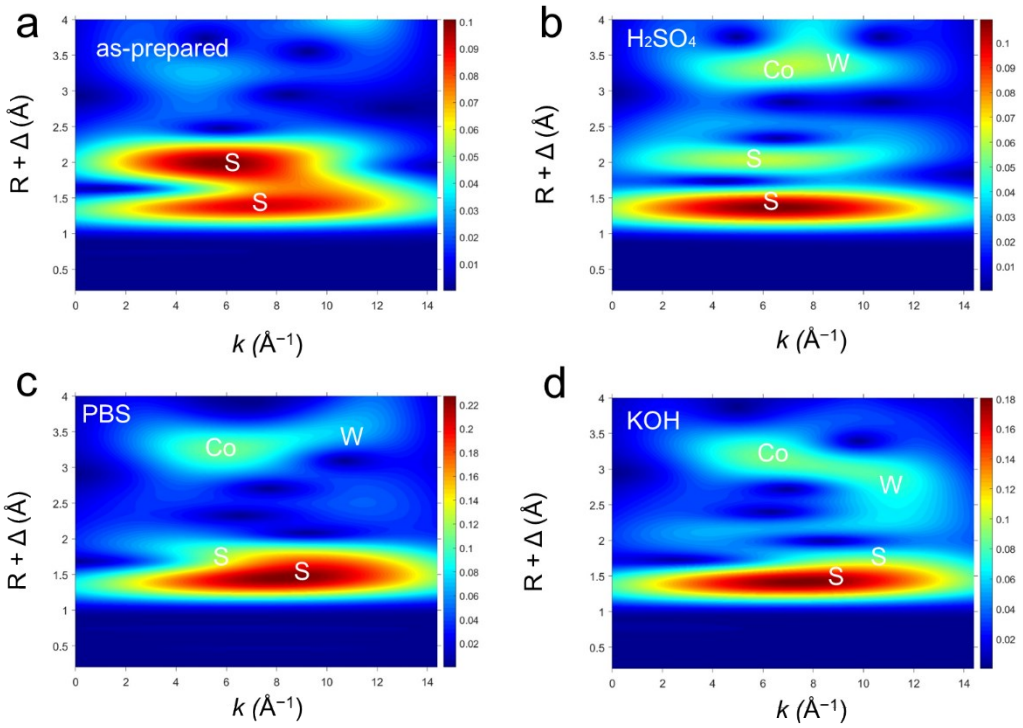

Fig. S12. The W-LIII wavelet transforms of (a) the as-prepared $Co_{0.5}W_{0.5}S_x$ and $Co_{0.5}W_{0.5}S_x$ after HER in (b) H_2SO_4, (c) PBS and (d) KOH electrolytes.

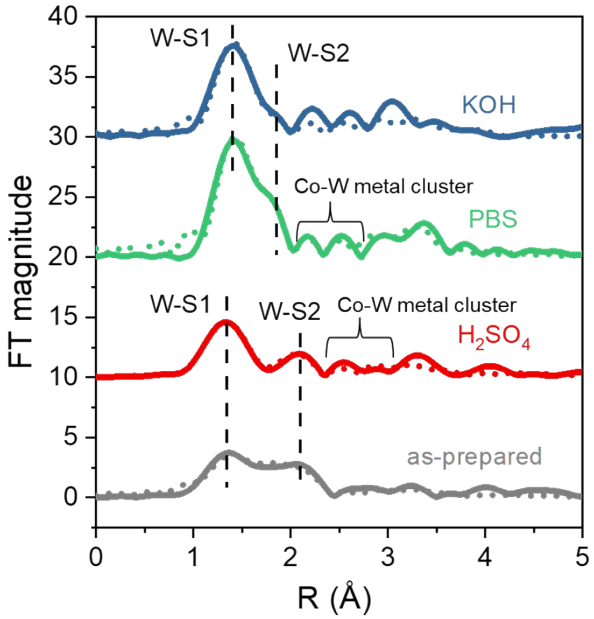

Fig. S13. The Fourier transformed k^3-weighted EXAFS data and the fits of $Co_{0.5}W_{0.5}S_x$ at W-LIII edge before and after HER. The spectra are not phase corrected.

Table S1. Representative elemental analysis of metal sulfide powders determined by EDS. Error values indicate the standard deviation between a minimum of 3 points on the sample surface.

Nominal composition	Found (at. %)	
	Co	W
$Co_{0.25}W_{0.75}S_x$	22±3	78±3
$Co_{0.5}W_{0.5}S_x$	52±3	48±3
$Co_{0.75}W_{0.25}S_x$	74±1	26±1

Table S2. Comparison of the HER performance of CoW-based catalysts.

catalyst	η_{10} (mV)	Tafel slope (mV dec^{-1})	Electrolyte	Reference
$Co_{0.5}W_{0.5}S_x$	200	83	0.5 M H_2SO_4	This work
$Co_{0.75}W_{0.25}S_x$	198	94	1 M PBS (pH 7)	This work
$Co_{0.5}W_{0.5}S_x$	189	127	1 M KOH	This work
Co-WP	98	51	0.5 M H_2SO_4	Appl. Catal. B 2019, 251 162–167
Co-WP	189	81	1 M PBS (pH 7)	Appl. Catal. B 2019, 251 162–167
Co-WP	119	55	1 M KOH	Appl. Catal. B 2019, 251 162–167
CoWS	250	74	0.5 M H_2SO_4	Appl. Surf. Sci. 2015, 341, 149-156
Co-W	> 200	146	30 wt% NaOH	Electrochim. Acta 2019, 318 597e606
Co/WN	208	92	0.5 M H_2SO_4	ChemCatChem 2020, 12, 2962–2966
Co/WN	161	92	1 M PBS (pH 7)	ChemCatChem 2020, 12, 2962–2966
Co/WN	151	82	1 M KOH	ChemCatChem 2020, 12, 2962–2966
Co-doped WS_2	160	76	0.5 M H_2SO_4	Sci. Rep. 2019, 9, 1357
$CoWS_x$	~ 250	78	0.1 M PBS (pH 7)	Energy Environ. Sci., 2013, 6, 2452–2459
Co_6W_6C-N@CNFs	50	85	0.5 M H_2SO_4	Int. J. Hydrogen Energy 2020, 45, 1901-1910
Co_6W_6C-N@CNFs	116	101	1 M KOH	Int. J. Hydrogen Energy 2020, 45, 1901-1910

Table S3. The model parameters of mean number of neighbours (N), refined distances (R) and Debye-Waller factors (σ^2) at Co-K edge. The error on co-ordination number and Debye-Waller factor are 15-25%. The parentheses values are standard deviations obtained from k^3-weighted least-squares refinements of the EXAFS function $\chi(k)$ and do not include systematic errors of the measurement.

As-prepared	**N (-)**	**R (Å)**	**σ^2 (Å^2)**	**$\Delta(E_o)$**
Co-S	3.892 (4)	2.312 (1)	0.005 (2)	-15.2 eV
Co-Co	1.481 (2)	3.054 (2)	0.007 (1)	
Co-W	0.363 (1)	3.285 (5)	0.018 (3)	
HER in H_2SO_4	**N (-)**	**R (Å)**	**σ^2 (Å^2)**	**$\Delta(E_o)$**
Co-S	3.812 (5)	2.315 (9)	0.006 (3)	12.2 eV
Co-Co	2.513 (3)	3.456 (8)	0.008 (5)	
Co-W	0.924 (2)	3.287 (6)	0.018 (7)	
HER in PBS	**N (-)**	**R (Å)**	**σ^2 (Å^2)**	**$\Delta(E_o)$**
Co-S	5.892 (5)	2.213 (2)	0.0112 (3)	-14.2 eV
Co-Co	5.213 (4)	3.156 (3)	0.0091 (4)	
Co-W	1.287 (7)	3.288 (6)	0.0122 (6)	
HER in KOH	**N (-)**	**R (Å)**	**σ^2 (Å^2)**	**$\Delta(E_o)$**
Co-S	5.992 (2)	2.196 (3)	0.0099 (6)	10.2 eV
Co-Co	8.213 (1)	3.137 (2)	0.0089 (5)	
Co-W	1.987 (2)	3.256 (1)	0.0195 (6)	

Table S4. The model parameters at W-LIII edge. The error on co-ordination number and Debye-Waller factor are 25%. The parentheses values are standard deviations obtained from k^3-weighted least-squares refinements of the EXAFS function $\chi(k)$ and do not include systematic errors of the measurement.

As-prepared	**N (-)**	**R (Å)**	**σ^2 (Å^2)**	**$\Delta(E_o)$**
W-S1	3.893 (3)	1.913 (1)	0.009 (6)	
W-S2	1.482 (2)	2.054 (5)	0.017 (5)	
W-Co	0.361 (5)	3.085 (4)	0.018 (5)	-8.2 eV
W-W	0.862 (2)	3.196 (3)	0.021 (4)	
HER in H_2SO_4	**N (-)**	**R (Å)**	**σ^2 (Å^2)**	**$\Delta(E_o)$**
W-S1	4.194 (8)	1.911 (3)	0.008 (7)	
W-S2	2.156 (6)	2.054 (2)	0.011 (3)	
W-Co	0.564 (5)	3.086 (1)	0.013 (2)	-7.2 eV
W-W	0.962 (3)	3.198 (5)	0.019 (1)	
HER in PBS	**N (-)**	**R (Å)**	**σ^2 (Å^2)**	**$\Delta(E_o)$**
W-S1	4.101 (4)	1.912 (1)	0.008 (3)	
W-S2	2.013 (4)	2.056 (5)	0.016 (2)	
W-Co	0.561 (3)	3.085 (7)	0.019 (2)	-5.2eV
W-W	0.962 (2)	3.192 (6)	0.021 (5)	
HER in KOH	**N (-)**	**R (Å)**	**σ^2 (Å^2)**	**$\Delta(E_o)$**
W-S1	4.123 (2)	1.951 (3)	0.008 (8)	-3.2eV

W-S2	2.112 (3)	2.098 (2)	0.019 (7)	
W-Co	1.063 (5)	3.087 (6)	0.021 (4)	
W-W	1.062 (7)	3.196 (5)	0.025 (5)	

References

1. I. J. George, G. N. Pickering, *EXAFSPAK*: A Suite of Computer Programs for Analysis of X-ray Absorption Spectra, SSRL, Stanford University, Stanford, CA, 1993.

2. S. I. Zabinsky, J. J. Rehr, A. Ankudinov, R. C. Albers, M. J. Eller, *Phys. Rev. B* 1995, **52**, 2995.

3. T. Verdonck, P. Verpoort, J. De Strycker, A. De Cleene, D. Banerjee, P. Nockemann, R. Van Deun, K. Van Hecke, *Dalton Trans.* 2019, **48**, 2318-2327.

4. K. P. J. Gustafson, A. Guðmundsson, É. G. Bajnóczi, N. Yuan, X. Zou, I. Persson, J.-E. Bäckvall, *Chem. Eur. J.* 2020, **26**, 3411-3419.

5. M. Filez, E. A. Redekop, H. Poelman, V. V. Galvita, G. B. Marin, *Anal. Chem.* 2015, **87**, 3520-3526.

6. M. Munoz, P. Argoul, F. Farges, *Am. Mineral.* 2003, **88**, 694–700.

7. M. Munoz, F. Farges, P. Argoul, *Phys. Scr. T.* 2005, **T115**, 221–222.